

DORV Fluid Dynamics

Analysis of the distribution and orientation of oxygenated and non-oxygenated blood in a Double Outlet Right Ventricle

D. Collia,¹ E. Angeli,² L. Careddu,² and G. Pedrizzetti¹

¹Department of Engineering and Architecture, University of Trieste, Trieste, Italy.

²Pediatric Cardiac Surgery and Adult Congenital Heart Disease Program, Department of Cardio-Thoracic and Vascular Medicine, IRCCS Azienda Ospedaliero-Universitaria di Bologna, Bologna, Italy.

(*Electronic mail: dario.collia@dia.units.it)

(Dated: 9 August 2023)

Double outlet right ventricle (DORV) is a malformation of the fetal heart in utero that affects the ventricular chambers. It usually presents with displacement of the aorta and more than half the circumference of both arterial valves in the right ventricle (RV). A peculiar characteristic is given by an interventricular septal defect (VSD) which allows communication between the left ventricle (LV) and the right with consequent mixing of oxygenated and non-oxygenated blood inside the cavities. A crucial question in assessing the degree of severity of functional dysfunction concerns the percentage of oxygenated blood that is ejected into the primary circulation via the aorta, a result which depends on the details of the vortex flow pattern within the two ventricular chambers. This study analyzes a complete DORV case through the use of numerical simulations that allow to identify the concentrations of oxygenated and non-oxygenated blood passing through this geometry. Results show that the VSD presents a significant impact on the fluid dynamic performance of the two ventricles. The analysis of blood concentration allowed to quantify the presence of oxygenated blood ejected into the pulmonary artery and of non-oxygenated blood into the aortic artery. The analysis of this specific case aim to demonstrate how the fluid dynamics analysis of this rare malformation, properly coupled with imaging technology, can provide information that could not be obtained otherwise and that are relevant for a careful clinical management including timely therapeutic intervention.

I. INTRODUCTION

The human heart is composed of a left and a right side. The two sides, which operate in approximate synchrony, are composed respectively of an atrium and a ventricle. The left ventricle (LV) receives oxygenated blood during diastole which will then be pumped into the aorta during its systolic phase. The right ventricle (RV), instead, receives non-oxygenated blood that will be pumped into the pulmonary artery during systole. Although both ventricles pump the same amount of blood, the LV is more powerful and presents a thicker myocardial muscle than the RV, because it develops the high pressure required for the systemic circulation, whereas resistances along the pulmonary circulation are smaller.

The timeline of human heart development remains partly elusive. Heart development begins as early as the third week of gestation and it assumes its characteristic four-chamber appearance by approximately 56 days of gestational age (DGA), while tissue architecture and organization is developing between 95 and 143 DGA¹. The transition from fetal to neonatal circulation is considered a period of intricate physiological, anatomical and biochemical changes in the cardiovascular system, in fact it is from a failure in fetal development that the congenital heart defect called Double Outlet Right Ventricle (DORV) develops.

DORV is a malformation of the fetal heart in the uterus that is characterized by presenting the two main arteries, the aorta and the pulmonary artery, originating both from the RV due to the displacement of the aorta toward the right side. DORV is rare and the causes are unclear, in some cases it happens to babies who have defects within their chromosomes². It occurs in approximately 4–8/1000 newborns and, by conservative es-

timates, it accounts for about 1–3% of all congenital heart defects^{2,3}. Symptoms of DORV usually appear during the first days or weeks after birth, although sometimes the defect can be found before birth using fetal echocardiography. DORV is always associated with a ventricular septal defect (VSD), an opening in the interventricular septum that puts the two ventricles in communication and allows blood to drain from the LV into the RV. The DORV is classified into several sub-types depending on the positioning of the VSD relative to the arterial positions.

Due to this malformation, the direct communication between pulmonary and aortic arteries leads to an increase of pressure in the pulmonary circulation that can damage the lungs. However, the principal criticality is due to the oxygenated and non-oxygenated blood that mix inside the RV, which can eject part of the oxygenated blood in the lungs and, importantly, a significant amount of non-oxygenated blood in the systemic circulation. This incorrect division of the flow can damage lungs, tissues and various organs and, in some cases, endanger life support. In fact, most children with DORV require heart surgery within the first year of life. The degree of severity to which the pathology reflects in the immediate cardiovascular function depends crucially on the relative oxygen distribution between the pulmonary and systemic circulations. An outcome that depends on the details of the vortical flow pattern that develops inside the two-ventricles domain.

This study analyzes a typical DORV case with non-committed VSD whose the distance between the VSD and the arterial valves is at least equal to the matched aortic valve diameter of the patient under study⁴. Through the use of numerical simulations we aim to identify the arrangement of oxygenated and non-oxygenated blood transiting through the RV

DORV Fluid Dynamics

| | $EDV[cm^3]$ | $ESV[cm^3]$ | $SV[cm^3]$ | $EF[\%]$ |
|----|-------------|-------------|------------|----------|
| LV | 1,73 | 1,07 | 0,66 | 38 |
| RV | 3,71 | 2,30 | 1,41 | 38 |

TABLE I. Volumetric values of the two ventricles. EDV =End Diastolic Volume, ESV =End Systolic Volume, SV =Stroke Volume= $EDV - ESV$, EF =Ejection Fraction= $\frac{SV}{EDV}$.

and across the two outlets, this could be represents a first step for the feasibility of a process that may help with the definition of most appropriate therapeutic direction, the most suitable type and timing of intervention or clinical management.

II. MATERIALS AND METHODS

A. Geometries

The analyzed pediatric case refers to a 5 day old non-operated subject. The geometric information was provided in anonymous form for post-processing in the context of a clinical study that was approved by the Institutional Review Board of the University Hospital of Bologna, all participants or their guardians provided informed consent to the usage of data in anonymous form for scientific research. The time-varying geometry of the two ventricular chambers was extracted from 3D-transesophageal echocardiography (TEE); the moving boundaries of the ventricular cavities are obtained by a semi-automatic procedure through dedicated software (4D LV-Analysis, 4D RV-Function; Tomtec Imaging Systems GmbH, Unterschleissheim, Germany) that also identifies the size and location of the valves. The clinical images were recorded with a time resolution of 21 images per heartbeat. Image processing analysis produced a triangulated surface of the moving geometry where vertices identify material points and their velocity is obtained from temporal differentiation. The main geometric information of the two ventricles are reported in table I. It is easy to see that LV is hypoplastic, much smaller than RV, with a different stroke volume (SV). The case analyzed is with non-committed VSD as it is located toward the apical region distant from aorta and pulmonary artery. The VSD is of the "severe" type, being of average diameter of VSD equal to $0,68cm^{5,6}$ and exceeding 75% of the diameter of the aortic annulus⁷ equal to $0,66cm$, the dimensions are obtained directly from the images. The close positions of the aortic valve (AV) and pulmonary valve (PV) make them identifiable as a "side by side" type.

The geometry of the mitral valve (MV), at the inlet of LV, is obtained in the fully open (at peak diastole) and fully closed (during initial systole) from TEE images and extracted through a dedicated software (4D MV-Assessment; Tomtec Imaging Systems GmbH, Unterschleissheim, Germany). The mechanical properties of the valvular tissues, as well as their geometric details, cannot be measured *in vivo*, limiting the possibility of a reliable mechanical analysis; to overcome this limitation, the geometry is allowed to span between the two

limiting positions, and the intermediate geometric configurations are reconstructed considering the two leaflets as moving independently, each one describing one degree of freedom associated with the opening angle, say $\varphi_1(t)$ and $\varphi_2(t)$, for the anterior and posterior leaflets, respectively. The valve geometry at a generic configuration is thus described by its coordinates $\mathbf{X}_{MV}(\vartheta, s, \varphi_1, \varphi_2)$, which represents a two-dimensional set of geometries associated with the two degrees of leaflets openings. This allows the two leaflets of the MV to assume different degrees of opening, for φ_1 and φ_2 respectively, starting from 0 (valve fully closed) up to $\frac{\pi}{2}$ (valve fully open). Therefore, this set of geometries is estimated by interpolation between $\mathbf{X}_{MV}(\vartheta, s, 0, 0)$, and $\mathbf{X}_{MV}(\vartheta, s, \frac{\pi}{2}, \frac{\pi}{2})$ configurations obtained from images as previously described⁸.

A tool for the extraction of the tricuspid valve (TV), at the inlet of the RV, from medical images is not available; therefore, the TV was described by a mathematical model in terms of the three degrees of freedom represented by the opening of each of the three leaflets. In this model, the three closed leaflets are assumed identical in a planar (closed) configuration, and each cusp opens along a circular trajectory and the geometry is built to connect the apex to the base with a quadratic profile ensuring continuous (horizontal) derivative at the annulus. This valve surface is then accommodated to lay over the bi-linear surface matching the curved annulus. Following the same line used for the MV, the TV is described by its coordinates $\mathbf{X}_{TV}(\vartheta, s, \varphi_1, \varphi_2, \varphi_3)$ where the three angles $\varphi_1, \varphi_2, \varphi_3$ correspond to the opening angle for each of the three leaflets, moving independently between 0 and $\frac{\pi}{2}$. These valvular models were a viable option based on patient-specific information for reproducing the individual main features of intraventricular fluid dynamics. The outlet valves, aortic and pulmonary, are described with a binary behavior, fully open or fully closed. The relative position of the valves and the VSD in the ventricular geometries is identified by the TEE image coordinates and does not require explicit registration. The complete 3D geometry of the examined case is shown in figure 1 with the respective volume curves of the two ventricles, (a) 3D without transparency, (b) 3D transparent with VSD highlighted. As it is possible to see in figure 1, a substantial difference compared to a healthy case is, in addition to the presence of the VSD, also the presence of AV in RV instead of in LV which substantially modifies the distribution of blood^{9,10} as indicated by the arrows in the figure and as we will specify in detail in the following sections.

B. Fluid Dynamics

The intraventricular fluid dynamics is evaluated by numerical solution of the Navier–Stokes and continuity equations

$$\frac{\partial \mathbf{v}}{\partial t} + \mathbf{v} \cdot \nabla \mathbf{v} = -\nabla p + \nu \nabla^2 \mathbf{v}, \quad (1)$$

$$\nabla \cdot \mathbf{v} = 0; \quad (2)$$

where $\mathbf{v}(t, \mathbf{x})$ is the velocity vector field, $p(t, \mathbf{x})$ is the kinematic pressure field, and ν is the kinematic viscosity (assumed

DORV Fluid Dynamics

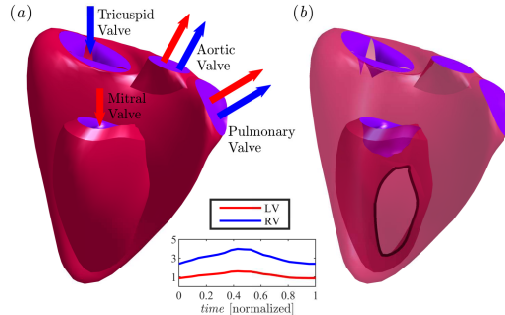


FIG. 1. (a) DORV geometry with TV and MV in semi-open position and AV and PV closed. (b) DORV with ventricular walls transparency showing the location of the VSD (marked in black). The volume curves of LV and RV are shown in the center of the figure in red and blue color respectively. The nomenclature of the valves are present in the figure together with a sketch indicating the direction of the inflow blood flow through red arrows for the oxygenated blood of LV blue for the non-oxygenated blood of RV and mixed in outflow through AV and PV.

$0.04 \text{ cm}^2/\text{s}$). Blood is intentionally assumed as a Newtonian fluid being the blood a mixture of elastic corpuscular elements in an aqueous solution and then either Newtonian or non-Newtonian models are approximate⁸. However, the influence of corpuscular or non-Newtonian behavior is very small in the heart chambers¹¹ and it is negligible when compared with the limited accuracy of the clinical data used as input.

The numerical method was described and validated for cardiac flow applications in a previous methodological study⁸; the main points are summarized below.

The solution is achieved by the immersed boundary method previously used in numerous studies^{8,9,12-16}, implemented with Matlab software (R2023) (MathWorks, Natick, U.S.A.) which we will recall here briefly. The equations are solved numerically in a bi-periodic Cartesian domain where spatial derivatives are approximated by second-order centered finite differences. Time advancement is achieved using a fractional step method in combination with a third-order Runge–Kutta explicit scheme. Boundary conditions are set on the moving immersed boundaries that comprise the ventricle geometry and valves surface, four cylindrical regions are added to the geometry extending from a region around the MV and TV (representing the surrogates of left and right atrium respectively) and a region around the AV and PV (representing the surrogates of pulmonary and aortic arteria), included for numerical convenience to avoid interference between the outflow and the inflow outside the geometry. The dynamics of the valvular leaflet is evaluated in the limit condition of no explicit resistance other than complying with the set of geometry obtained from medical imaging; individual leaflets' movement is obtained by the kinematic condition that the motion of the leaflet surface must match the velocity of the fluid at the same position. This is imposed in the least square sense, in integral

form over each individual leaflet, and gives rise to system of dynamic equation for the advancement of each leaflet opening angle. This procedure, described in details in⁸, results in a system of linear equations whose i th term reads

$$\left[\int_{A_v} \left(\frac{\partial \mathbf{X}_v}{\partial \varphi_i} \cdot \mathbf{n} \right) \left(\frac{\partial \mathbf{X}_v}{\partial \varphi_j} \cdot \mathbf{n} \right) dA \right] \frac{d\varphi_j}{dt} = \int_{A_v} (\mathbf{v} \cdot \mathbf{n}) \left(\frac{\partial \mathbf{X}_v}{\partial \varphi_i} \cdot \mathbf{n} \right) dA; \quad (3)$$

where \mathbf{n} is the normal to the valvular surface and the subscript v stands for either MV or TV (summation over j is implicit and extends to 2 or 3 for the mitral and tricuspid valve, respectively). The aortic and pulmonary valves are considered open when the tricuspid and mitral valves are closed and normal velocities, averaged over the position of the aortic and pulmonary valve surface respectively, before establishing boundary conditions, are directed outward. In this way, the open or closed state of the valve is automated and does not require to be imposed⁸.

C. Flow Transit Analysis

Flow transit assessment is an important step in identifying the transport of oxygenated and non-oxygenated blood from LV to RV and vice versa. The aim is to independently follow the blood volumes originating from LV and RV to identify their journey throughout the entire heartbeat. These quantities are defined through blood transport analysis that is performed by solving the transport-diffusion equation for a passive scalar

$$\frac{\partial C}{\partial t} + \nabla \cdot (\mathbf{v}C) = D\nabla^2 C, \quad (4)$$

where $\mathbf{v}(\mathbf{x}, t)$ is the know velocity field, D is the diffusive coefficient that is set equal to the kinematic viscosity of blood to reproduce blood diffusion and $C(\mathbf{x}, t)$ is the total concentration of particles. Equation (4) is solved separately for the LV and for the RV in parallel to the Navier–Stokes equation (1) starting from the initial condition $C(\mathbf{x}, 0) = 1$ in the interior of the ventricle at beginning of diastole. Since equation (4) is solved separately for LV and RV, there is a C field for each ventricle that allows to trace the two different blood concentrations, oxygenated in LV and non-oxygenated, and their mixing within the entire RV-LV domain.

When performing global blood balance it is necessary to compute the flow rate that crosses each ventricular opening, the four valvular orifices and the VSD. The overall flow rate is obtained from the relative fluid velocity, \mathbf{v}_{rel} , at the orifice

$$Q(t) = - \int_A \mathbf{v}_{rel} \cdot \mathbf{n} dA, \quad (5)$$

where the minus sign follows from the fact that \mathbf{n} is the outward unit normal vector, so that the flow rate is positive when it enters the ventricle. The extension of equation (5) that includes the concentrations C allows to differentiate between oxygenated and non-oxygenated blood flow rate

$$Q_C(t) = - \int_A \mathbf{v}_{rel} \cdot \mathbf{n} C dA. \quad (6)$$

DORV Fluid Dynamics

4

The corresponding volumes are then obtained as the time integral of the flow rate in the reference period (i.e. systole and diastole), which can be either the forward volume or the regurgitated back flow.

D. Kinetic Energy and Vortex Formation Time

The kinetic energy (KE) of blood reflects a fundamental component of the work done by the two ventricles, indicated as the movement of the blood within them^{17,18}, and it is computed as follows

$$KE(t) = \frac{\rho}{2} \int_V v^2 dV, \quad (7)$$

where $V(t)$ is the ventricular volume and ρ the blood density. The vortex formation time (VFT) is an important parameter used for the evaluation of ventricular functions¹⁹; this dimensionless parameter is computed as

$$VFT = \int_{T_E} D^{-1} v_{or} dt, \quad (8)$$

where v_{or} is the mean velocity across the valvular orifice¹⁴⁻¹⁶, D the average diameter, and T_E is the diastolic E-wave period. This parameter measures the quality of the vortex formation process and optimal both LV and RV filling.

E. Blood Oxygen Saturation

An important parameter capable of providing information on the efficiency of oxygen transport in the blood is oxygen saturation, S_aO_2 , defined as the ratio of between the oxygen content (O_2) in the blood, neglecting the amount of oxygen physically dissolved in the blood which has a value of less than 1% of the total²⁰, and the O_2 transport capacity of hemoglobin (H_b):

$$S_aO_2 = \frac{H_b O_2}{H_b + H_b O_2} \cdot 100. \quad (9)$$

This parameter is considered an excellent indicator of the efficiency of the blood oxygenation system. Optimal values are between the range of 94%÷100%²¹. Through equation 6 we can identify the parameters useful for calculating S_aO_2 : the quantities of oxygenated blood (AV_{OX} , PV_{OX}) which are the equivalent of $H_b O_2$, the non-oxygenated quantities (AV_{NOX} , PV_{NOX}) which are the equivalent of H_b . The inverse calculation makes it possible to identify the non-oxygenated quantities ejected into the two orifices. The result of this equation therefore allows to identify the quality of blood effectively ejected from the two orifices.

F. An Additional Constrain on Blood Flow Balances

Before moving to the results, it is necessary to make an additional consideration on the blood balances during the entire

| | ΔV_{MV} | ΔV_{TV} | ΔV_{PV} | ΔV_{AV} | ΔV_{VSD} |
|----|-----------------|-----------------|-----------------|-----------------|----------------------|
| LV | +0.66 | - | - | - | -0.66 (+0.01 - 0.67) |
| RV | - | +1.41 | -0.68 | -1.39 | +0.66 (-0.01 + 0.67) |

TABLE II. Blood volumes, in cm^3 , exchanged by the two ventricles over one heartbeat.

ΔV_{MV} =blood volume crossing the MV, ΔV_{TV} =volume crossing the TV, ΔV_{PV} =volume crossing the PV, ΔV_{AV} =volume crossing the AV, ΔV_{VSD} =volume crossing the VSD (in parenthesis the values separated for diastole and systole).

cardiac cycle. The fundamental principle to be satisfied is the principle of mass conservation in the complete system that includes both ventricles where the quantity of blood (stroke volume, SV) that enters during the inflow phase (diastole) must be the same that leaves during the outflow (systole). This global conservation is automatically satisfied by the fulfilment of equation (2).

In the DORV condition, due to the connection between the two ventricles an additional consideration must be made to take into account that the PV and AV are in series with the MV and TV, respectively. This point would be satisfied by a model of the entire circulation that, however, requires a series of additional elements that are of difficult evaluation at an individual level. In the present model, this point requires the fulfilment of an additional constrain ensuring that the net volume (ΔV_{MV}) entering the LV across the MV during diastole balances with that expelled during systole from the RV across the PV ($\Delta V_{MV} = \Delta V_{PV}$), and that entering the RV across the TV balances with that ejected through the AV ($\Delta V_{TV} = \Delta V_{AV}$); where each ΔV_* is the time integral of the corresponding $Q(t)$ evaluated by equation (5). This constraint is verified by inserting one resistances at the PV, or at the AV, to control the relative partition during of systolic ejection. In this study a resistance on the PV was introduced, simply by reducing the orifice size, which allowed us to correctly balance the two outputs; the different volumetric contributions are reported in table II.

It is important to remark that DORV patients may be subjected to valve regurgitation (backflow) across either the MV or the TV during diastole even in absence of a pathological valvular insufficiency (that would give regurgitation during systole, instead); therefore, these values represent the net volumetric exchange including the negative contribution of diastolic "false regurgitation"¹⁴.

III. RESULTS

The fluid dynamics in the normal LV and RV has been extensively described in the literature^{9,10}. The blood flow entering the LV from MV moves along the posterior wall generating a rotational movement that expands throughout the ventricle until it is redirected towards the aortic output. Instead in RV the incoming flow from TV stays in the region below the valve and then converges towards the pulmonary outlet tract. This picture is modified in DORV due to several factors

DORV Fluid Dynamics

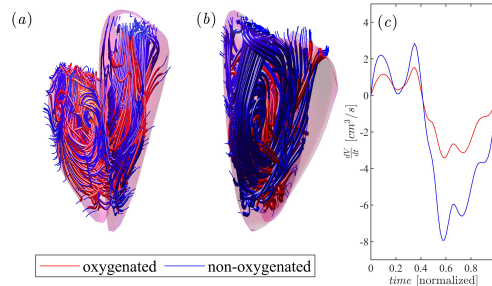


FIG. 2. Streamlines of the steady-streaming (diastolic phase-average) - (a) DORV lateral view - (b) back RV view, (c) Curves of dV/dt respectively for LV (red line) and RV (blue line).

such as the VSD opening, that allow blood flowing between the two ventricles, and the localization of both outlets in the RV. In figure 2 (a), we show this phenomenon from a diastolic point of view, the oxygenated blood enters the ventricle and mixes rotationally with the non-oxygenated blood entering from the VSD. This movement is unusual for the diastolic phase^{8,14-16}, thus showing a substantial fluid dynamic modification within the LV. The same is for RV, the presence of the VSD and the entry of oxygenated blood into it substantially modifies its distribution which under normal conditions is predominantly in its posterior section near the apex⁹ and not as extensive as shown in figure 2 (b).

The global exchanges of blood flow in the DORV during the cardiac cycle are summarized in figure 3, whose integrated value correspond to figures reported in table II. Panel (a) reports the flow rate, $Q(t)$, crossing the 4 valves during inflow (diastole) and outflow (systole); panel (b) shows the blood flow rate passing from one ventricle to the other through the VSD and where, by convention, the negative part (red color) represents the oxygenated blood which moves from the LV to the RV and the positive part (blue) is the non-oxygenated blood moving in the opposite direction.

During the initial phase of the diastolic filling the flow rapidly enters the two ventricles (figure 3a), as dictated by individual ventricular expansion; in this phase blood exchanged through the VSD is mostly oxygenated (from LV to RV) to comply with the limited volume of hypo-plastic LV. Afterwards, during the second phase of the filling, the two ventricles enter more in equilibrium, they continue their regular filling and a limited quantity of non-oxygenated blood flows across the VSD; the final part of diastole ($t \approx 0.42s$) features the development of a false regurgitation (outflow during diastole) of blood across both MV and TV. Therefore, during diastole, a quantity of blood equal to the SV (table I) enters the ventricles for LV and RV respectively, there is an exchange of blood through the VSD and finally some is lost by regurgitation; these quantities are shown in the table II.

Note that the inlet flow rates are calculated at the valve end leaflet where in "normal" cases, i.e. without VSD and valve

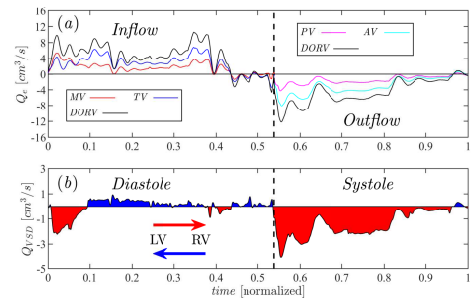


FIG. 3. (a) Curves of blood Inflow and Outflow across the four valves: MV (red color), TV (blue), PV (magenta), AV (cyan); the black curve reports the total for the entire DORV. (b) Flow exchange between LV and RV through the VSD as send from the LV: negative value corresponds to flow from LV to RV reported in red color (oxygenated blood), positive is flow from RV to LV in blue color (non-oxygenated blood).

regurgitation, the flow is more linear¹⁴. In DORV cases, on the other hand, the fluid dynamics modification causes a different flow recirculation than usual, there is an exchange of blood flow from the VSD which generates substantial modifications with a return of flow in the proximity of the two valves which are detected by the end leaflets being inside the ventricle without affecting the valve dynamics (3 (c)). The dV/dt curves in figure 2 (c) are calculated directly from the volumes of the geometries through a dedicated software that does not take into account these observations since they are structural anomalies from malformation. What has been said is confirmed by the data in table II calculated through the flow rate which are perfectly comparable to those in table I extracted from the geometry.

During systole, the RV ejects blood into the two outlet orifices, PV and AV, while the LV contraction pushes blood to the right side across the VSD. Therefore, as systole begins, the mostly non-oxygenated blood that resides in the RV immediately begins to flow out of the two valves while oxygenated blood enters the RV and mixes therein. As systole progresses, blood flows out the two orifices with an increasing percentage of oxygenated flow, as shown in figure 4 (c) and (d), that reaches a peak at time $t \approx 0.76s$ and progressively decreases to the end of systole. Figure 4 shows the steady-streaming (systolic average) streamlines in front and back views, panel (a) and (b), respectively. The front view indicates the directions of the non-oxygenated blood which is immediately oriented towards the two outlets, the back view shows how the oxygenated blood entering the RV initially travels to the posterior section of the ventricle where a part remains inside the RV and a part mixes with the non-oxygenated blood directed towards the two outlets.

The presence of an underdeveloped LV implies that the amount of oxygenated blood is lower than the non-oxygenated and that the outflow in the PV to the pulmonary circulation is

DORV Fluid Dynamics

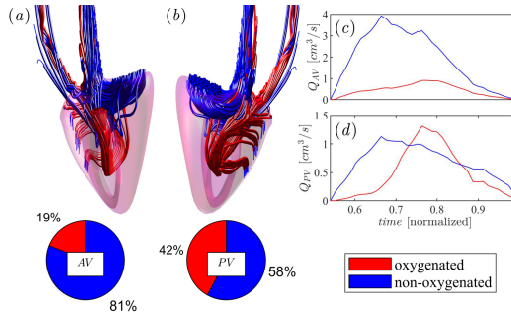


FIG. 4. Streamlines of the steady-streaming (systolic phase-average) - (a) front view - (b) back view, (c) Curves of outflow blood in AV, (d) Curves of outflow blood in PV. Red color represent the oxygenated blood, blue color the non-oxygenated blood. The lower section of the figure shows a pie graph with the percentage of blood quality ejected through AV and PV.

| | AV _{OX} | AV _{nOX} | PV _{OX} | PV _{nOX} |
|-------------------|------------------|-------------------|------------------|-------------------|
| $\Delta V [cm^3]$ | 0.26 | 1.13 | 0.29 | 0.39 |

TABLE III. Composition of blood ejected in AV and PV during systolic phase. The acronym OX identifies oxygenated blood, nOX non-oxygenated blood.

lower than in the primary circulation.

Within this picture, table III shows the quantities of oxygenated and non-oxygenated blood crossing the two outlets. The first observation (calculated with equation 9) is that not all the oxygenated blood entering the RV comes out of the two orifices but only 82% while the remaining 16% is trapped inside the RV. This does not mean that less total blood is ejected, but that the 16% trapped during the mixing phase is "replaced" by the same non-oxygenated amount present in RV. Thus, at end systole, the residual blood volume in the RV is a mix of oxygenated and non-oxygenated blood. The quality of blood ejected from the two orifices is also shown in the lower section of figure 4. From the percentage subdivision we note that the AV has a dominance of non-oxygenated blood ejected compared to oxygenated (81% vs 19%) while in PV the percentages are more evenly distributed (58% vs 42%). The quantity and quality of blood expelled from the two orifices tells us that of about half of the oxygen ends up in the primary circulation and a little more returns in lungs.

A calculation of total oxygen saturation shows a $S_aO_2 = 26\%$ value coherent with DORV cases that are typically cyanotic^{22,23} and with more severe hypoxic problems²⁴ such as the one examined in this study.

In figure 5 we show the trend of KE during the entire heart-beat for both LV (KE_{LV}) and RV (KE_{RV}) respectively normalized with own SV. This orientation confirms what has been said so far also from an energy point of view. The time course of KE_{LV} increases more rapidly than KE_{RV} reaching a greater

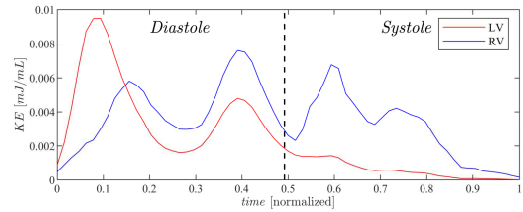


FIG. 5. Kinetic Energy curves in DORV. The KE time course are shown in red and blue color respectively for LV and RV.

| | VFT | $KE_{E_{peak}}$ | $KE_{A_{peak}}$ | $mean KE_{dia}$ | $mean KE_{sys}$ |
|----|-----|-----------------|-----------------|-----------------|-------------------------|
| LV | 0.5 | 0.0094 | 0.0048 | 0.0042 | $8.4136 \cdot 10^{-04}$ |
| RV | 0.6 | 0.0058 | 0.0076 | 0.0041 | 0.0031 |

TABLE IV. Vortex formation Time is an adimensional value. Kinetic Energy is expressed in mJ/mL .

VFT=Vortex Formation Time value, $KE_{E_{peak}}$ =KE value at E-wave peak, $KE_{A_{peak}}$ =KE value at A-wave peak, $mean KE_{dia}$ =Averaged diastolic KE, $mean KE_{sys}$ =Averaged systolic KE.

value at the peak of E-wave. This is related to the first predominant inflow of oxygenated blood into the RV via the VSD during early diastolic and then to a greater initial thrust as we can see in figure 3 (b). Subsequently, during diastasis phase it decreases very quickly unlike KE_{RV} which maintains a more constant energy level until it increases at the peak of A-wave (atrial thrust) which is greater in RV. The result of this left atrial thrust matches the second entry of oxygenated blood into the RV, in a less predominant way being a suffering and hypotrophic ventricle. RV, on the other hand, reacts to this invasion with a dominant A-wave peak which forcefully directs the flow towards the systolic phase. During systole, oxygenated blood flows slowly from LV to RV due to poor LV performance which is mirrored in KE_{LV} where it slowly resets. In RV, on the other hand, it is interesting to see how this hypertrophic ventricle actually functions much more than the left; the presence of the double wave represents the energy increase respectively in AV and PV.

These KE curves show the additional severity of the malformation when compared with the literature. In a healthy adult heart, the diastolic trend follows an E-wave peak greater than the A-wave peak with $E/A > 1$ ²⁵. Instead, this is not the case for a heart from 0 to 1 month of life where peak A-wave is greater than E-wave with an $E/A < 1$ and then increases with age²⁶. Although our case falls within this series (E/A is 0.84 and 0.86 respectively for LV and RV), confirming the goodness of the data, the KE trend confirms the presence of effective left ventricular suffering which initially tries to push hard and then it is also lost due to the invasion of the RV in its diastolic phase if compared with children control case present in literature^{27,28}. In the systolic phase there is minimal energy in LV and a double curve in RV due to the double output, not consistent with a healthy heart but consistent with the DORV

series²³. In fact, the values in table IV also confirm what has been said with a great similarity to cases of adults with severe heart failure^{29,30}. The LV *mean* KE_{sys} value very close to zero is well associated with the description of how oxygenated blood actually flows slowly towards the RV to then be sucked up and mixed in the right circulation and finally expelled in the manner illustrated in figure 4, with particular attention to the curves of oxygenated blood expelled which slowly increase. This is also a consequence of the greater total amount of blood expelled in the AV compared to the PV²³ given also by the close position of the aortic valve to the VSD. A further value confirming what has been said so far is the VFT (table IV), an indicator of ventricular efficiency, which in this case DORV of a 5-day old child is low (0.5 and 0.6 for LV and RV respectively) when compared with control cases of infants aged between 0 and 1 month who generally present a value between 1 and 2²⁶. This great diastolic suffering is reflected, as we have seen, throughout the systolic phase, significantly influencing the distribution of blood in the DORV with consequent differences in blood concentration in the two outlets. In fact, the hypoplastic condition of LV, the ventricular suffering in both energetic and biomechanical terms, the presence of VSD and the poor blood distribution capacity affect the low blood saturation obtained.

IV. CONCLUSIONS

Hearts with DORV are a heterogeneous group of malformations in which a comprehensive diagnostic approach is required for tailored surgical management³¹. In this malformation, the VSD plays an essential role to drain the LV, it represents a short-circuit between pulmonary and systemic circulations that alters their serial arrangement; thus its structure influences the qualitative redistribution of blood in the two ventricles that can only be evaluated by a careful analysis of intra-ventricular fluid dynamics.

In this study we analyzed a 5 day old DORV pediatric case, non operated and with non-committed VSD through a well-validated and consolidated numerical simulation method^{8,11}. This method offers optimal resolution and computational detail for post-processing^{8-10,14-16,32-34} would not be possible with other evaluation methods. An example is the 4D Flow MRI which, on the one hand, would have the advantage of being an effective measurement on the patient; on the other, MRI has a low spatial and temporal resolution and does not capture small vortices that are important for the dispersion phenomena and may not allow to identify in detail the effective blood distribution. Moreover, the work for post processing of 4D Flow MRI data would be comparable to that required for a numerical simulation. The use of numerical simulations makes it possible to obtain results with great detail and without further examination to the patient, considering that we are talking about young children. The numerical simulation, despite all its limitations, allows to highlight many clinical characteristics in greater detail using patient specific TEE images^{14,35,36}, moreover thanks to the new technologies it is possible to obtain 3D recording also thanks to simple

echocardiographic examinations^{10,37}, limiting the invasiveness and stress for the patient, making the coupled numerical simulation-3D echocardiography one of the better solutions currently proposed for different types of patient's specific clinical evaluations. Importantly, numerical simulation can, in perspective, allow to reproduce hypothetical condition that would occur in different therapeutical solutions opening the possibility to evaluate virtual surgery. Identification of blood oxygenation is vital for DORV cases. Among the first most important damages are brain lesions, a lack of oxygenated blood in the brain can create both white matter lesions and gray matter infarctions, occurring among the most common in children with severe VSD³⁸. After surgery, lesions seen on neonatal MRI usually resolve within 4-6 months³⁹, but neurodevelopmental delays remain for life thus increasing the risk of cognitive impairment. This is because this malformation affects brain growth from the beginning of gestation with a reduction in the volumes of the cortical and subcortical gray and white matter as early as 25 weeks of gestation⁴⁰, leading the newborns to have a clearly reduced head circumference⁴¹. In fact, in children with DORV, the incidence of motor dysfunction related to neurological dysfunction and poor tissue oxygenation also increases, with important consequences such as lower IQ scores, reduced expressive language, behavioral problems, reduced expressive language, self-esteem and academic competence around 7 years of school age^{42,43}.

The analysis in this specific case showed that the oxygenated blood that flows into the RV through the VSD is preferably redirected towards the pulmonary outflow tract than the aortic outlet. Moreover, the presence of an underdeveloped LV implies that a reduced amount of blood volume flows into the pulmonary circulation and that the availability of oxygenated blood in the DORV is overall reduced. As a result, the available oxygenated blood is approximately evenly distributed between the two outlets, while the non-oxygenated is principally ejected in the primary circulation.

The reduced oxygen content across the AV outlet decreases the oxygen supply to the tissues and limits the working capacity of the muscles, in agreement with clinical observation^{44,45}. The present analysis is largely retrospective in a subjected who underwent surgical operation and it has no clinical implication. Nevertheless, this type of analysis provides incremental information for a clinical decisions on therapeutic path and to avoid irreversible damage. These malformations are rare and therefore very little is known about them, so it is important to expand this knowledge, deepen existing cases in order to create a more immediate and systematic method of intervention given by greater knowledge both from a fluid dynamic and mechanical point of view.

Given the many known and unknown consequences due to the rarity of this malformation, this numerical method could also be used to identify the evolution of the malformation already at the fetal level, right from the first cardiac formation which usually occurs in DORV cases with certain genetic conditions, such as trisomy 13, trisomy 18 or DiGeorge syndrome⁴⁶⁻⁴⁸. This could help medicine understand how blood is distributed from its earliest moments and design new ways of intervening both before and after childbirth. More-

DORV Fluid Dynamics

over, this would be possible thanks to a non-invasive analysis such as the numerical simulation associated with 3D echocardiography.

These malformations of the fetal heart are very rare and this study intends to represent a clinical input to give greater knowledge both from a clinical point of view and from a surgical perspective.

V. LIMITATIONS

DORV is rare and this leads to have low data and analysis on this malformation. This rarity has led to the first limitation of this work that is the study of only one case. Despite this, however, it has allowed us to start a first detailed analysis of how the malformation could evolve regarding its blood distribution in the pulmonary and systemic circulation. This single study is not generalizable and this is a second limitation, as given the many combinations that this malformation can have both at the terms of the VSD and of the valves or ventricular conformation. However, this is a first step towards new future perspectives that push us to continue on this path, expanding the case studies even in an artificial way by building a parametric model that tries to summarize countless case studies that could occur in the DORVs. However, this remains a first clinical case, analyzed with this method, useful for giving detailed first clinical information on a specific patient DORV.

DATA AVAILABILITY STATEMENT

The raw data supporting the conclusions of this article can be made available by the authors under a confidentiality agreement.

AUTHORS CONTRIBUTION

All authors participated to conceiving the study, provided substantial contributions during its progress, revised the manuscript and approved it for publication. In particular, DC performed the calculations and drafted the first version of the manuscript; EA and LC acquired the medical data and supervised the clinical evaluations; GP participated to the calculations and supervised the overall study.

ACKNOWLEDGEMENTS

DC and GP acknowledge partial support by Italian Ministry of Education, University and Research under project PRIN 2017A889FP_006.

¹E. Pervolaraki, J. Dachtler, A. A. R., and A. V. Holden, "Ventricular myocardium development and the role of connexins in the human fetal heart," *Scientific Reports* **7**, 12272 (2017).

²D. Obler, A. L. Juraszek, L. B. Smoot, and M. R. Natowicz, "Double outlet right ventricle: aetiologies and associations," *J. Med. Genet.* **45**, 481–497 (2008).

³L. D. Botto and A. Correa, "Decreasing the burden of congenital heart anomalies: an epidemiologic evaluation of risk factors and survival," *Prog. Pediatr. Cardio.* **18**, 111–121 (2003).

⁴E. Belli, A. Serraf, F. Lacour-Gayet, M. Hubler, J. Zoghby, L. Houyel, and C. Planche, "Double-outlet right ventricle with non-committed ventricular septal defect," *European Journal of Cardio-Thoracic Surgery* **15**, 747–752 (1999).

⁵M. C. Vaillant, A. Chantepie, C. Cheliakine, M. Nashashibi, J. M. Pottier, and J. Laugier, "Contribution of two-dimensional echography in predicting spontaneous closure of interventricular defects in infants," (1992).

⁶O. Gomez, J. M. Martinez, A. Olivella, M. Bennasar, F. Crispi, N. Masoller, J. Bartrons, B. Puerto, and E. Gratacos, "Contribution of two-dimensional echography in predicting spontaneous closure of interventricular defects in infants," *Ultrasound Obstet. Gynecol.* **43**, 65–71 (2014).

⁷W. Dakkak and T. I. Oliver, *Ventricular Septal Defect* (Treasure Island (FL): StatPearls Publishing, 2022).

⁸D. Collià, M. Vukicevic, V. Meschini, L. Zovatto, and G. Pedrizzetti, "Simplified mitral valve modeling for prospective clinical application of left ventricular fluid dynamics," *J. Comput. Phys.* **398**, 108895 (2019).

⁹D. Collià, L. Zovatto, G. Tonti, and G. Pedrizzetti, "Comparative analysis of right ventricle fluid dynamics," *Front. Bioeng. Biotechnol.* **9**, 667408 (2021).

¹⁰D. Collià, G. Pedrizzetti, T. Sato, D. Matsubara, L. Zovatto, M. Gei, A. Banerjee, and G. Pedrizzetti, "Interplay between geometry, fluid dynamics, and structure in the ventricles of the human heart," *Phys. Rev. Applied* **3**, 3–3 (2022).

¹¹V. Meschini, M. de Tullio, G. Querzoli, and R. Verzicco, "Flow structure in healthy and pathological left ventricles with natural and prosthetic mitral valves," *J. Fluid Mech.* **834**, 271–307 (2018).

¹²G. Pedrizzetti, G. L. Cannà, O. Alfieri, and G. Tonti, "The vortex an early predictor of cardiovascular outcome?" *Nat. Rev. Cardiol.* **11**, 545–553 (2014).

¹³F. Domenichini, "On the consistency of the direct forcing method in the fractional step solution of the navier–stokes equations," *J. Comput. Phys.* **227**, 6372–6384 (2008).

¹⁴D. Collià, L. Zovatto, and G. Pedrizzetti, "Analysis of mitral valve regurgitation by computational fluid dynamics," *APL Bioeng.* **3**, 036105 (2019).

¹⁵D. Collià, "Mitral valve asymmetry in healthy, pathological, and repaired cases," *Phys. Fluids* **22**, 077118 (2021).

¹⁶D. Collià and G. Pedrizzetti, "The influence of mitral valve asymmetry for an improved choice of valve repair or replacement," *Fluids MDPI* **7**, 293 (2022).

¹⁷A. Fredriksson, A. Trzebiatowska-Krzyszka, P. Dyverfeldt, J. Engvall, T. Ebbers, and C. J. Carlhäll, "Turbulent kinetic energy in the right ventricle: Potential mr marker for risk stratification of adults with repaired tetralogy of fallot," *J. Magn. Reson. Imaging* **47**, 1043–1053 (2018).

¹⁸M. Carlsson, E. Heiberg, J. Töger, and H. Arheden, "Quantification of left and right ventricular kinetic energy using four-dimensional intracardiac magnetic resonance imaging flow measurements," *Am. J. Physiol. Heart. Circ. Physiol.* **302**, H893–H900 (2012).

¹⁹G. King, N. Ngiam, J. Clarke, M. J. Wood, and K. K. Poh, "Left ventricular vortex formation time in elite athletes," *Int. J. Cardiovasc. Imaging* **35**, 307–3011 (2019).

²⁰F. P. Branca, *Fondamenti di Ingegneria Clinica Volume 1* (Springer, 2005).

²¹R. Langley and S. Cunningham, "How should oxygen supplementation be guided by pulse oximetry in children: Do we know the level?" *Frontiers in Pediatrics* **4**, 138 (2017).

²²R. Ahmed, H. A. Hashmi, and B. Mora, "Lost in transition: a case report of very late palliation of a double outlet right ventricle," *European Heart Journal - Case Reports* **7**, 1–5 (2023).

²³H. Wiputra, C. K. Chen, E. Talbi, G. L. Lim, S. M. Soomar, A. Biswas, C. N. Z. Mattar, D. Bark, H. L. Leo, and C. H. Yap, "Human fetal hearts with tetralogy of fallot have altered fluid dynamics and forces," *Am. J. Physiol. Heart. Circ. Physiol.* **315**, H1649–H1659 (2018).

²⁴S. Sridaromont, R. H. Feldt, D. G. Ritter, G. D. Davis, and J. E. Edwards, "Double outlet right ventricle: Hemodynamic and anatomic correlations," *The American Journal of CARDIOLOGY* **38**, 85–94 (1976).

²⁵G. Faganello, D. Collià, S. Furlotti, L. Pagura, M. Zaccari, G. Pedrizzetti, and A. D. Lenarda, "A new integrated approach to cardiac mechanics: reference values for normal left ventricle," *The International Journal of Car-*

- diovascular Imaging **36**, 2173–2175 (2020).
- ²⁶A. Kulkarni, D. Morisawa, D. Gonzalez, and A. Kheradvar, "Age-related changes in diastolic function in children: Echocardiographic association with vortex formation time," *Echocardiography* **36**, 1869–1875 (2019).
- ²⁷P. Sjöberg, E. Heiberg, P. Wingren, J. R. Johansson, T. Malm, H. Arheden, P. Liuba, and M. Carlsson, "Decreased diastolic ventricular kinetic energy in young patients with fontan circulation demonstrated by four-dimensional cardiac magnetic resonance imaging," *Pediatr Cardiol* **38**, 669–680 (2017).
- ²⁸P. Sjöberg, J. Töger, E. Hedström, P. Arvidsson, E. Heiberg, H. Arheden, R. Gustafsson, S. Nozohoor, and M. Carlsson, "Altered biventricular hemodynamic forces in patients with repaired tetralogy of fallot and right ventricular volume overload because of pulmonary regurgitation," *Am J Physiol Heart Circ Physiol* **315**, H1691–H1702 (2018).
- ²⁹M. Kanski, P. M. Arvidsson, J. Töger, R. Borgquist, E. Heiberg, M. Carlsson, and H. Arheden, "Left ventricular fluid kinetic energy time curves in heart failure from cardiovascular magnetic resonance 4d flow data," *Journal of Cardiovascular Magnetic Resonance* **17**, 111 (2015).
- ³⁰A. Riva, F. Sturla, S. Pica, A. Camporeale, L. Tondi, S. Saitta, A. Caimi, D. Giese, G. Palladini, P. Milani, S. Castelvecchio, L. Menicanti, A. Redaelli, M. Lombardi, and E. Votta, "Comparison of four-dimensional magnetic resonance imaging analysis of left ventricular fluid dynamics and energetics in ischemic and restrictive cardiomyopathies," *J. Magn. Reson. Imaging* **56**, 1157–1170 (2022).
- ³¹D. Yim, A. Dragulescu, H. Ide, M. Seed, L. Grosse-Wortmann, G. van Arsdell, and S. J. Yoo, "Essential modifiers of double outlet right ventricle revisit with endocardial surface images and 3-dimensional print models," *Circulation: Cardiovascular Imaging* **11**, e006891 (2018).
- ³²D. Collià, G. Libero, G. Pedrizzetti, and V. Ciriello, "Surrogate models provide new insights on metrics based on blood flow for the assessment of left ventricular function," *Scientific Reports* **12**, 8695 (2022).
- ³³J. O. Mangual, E. Kraigher-Krainer, A. D. Luca, L. Toncelli, A. Shah, S. Solomon, G. Galanti, F. Domenichini, and G. Pedrizzetti, "Comparative numerical study on left ventricular fluid dynamics after dilated cardiomyopathy," *J Biomech.* **46**, 1611–1617 (2013).
- ³⁴G. Pedrizzetti and F. Domenichini, "Left ventricular fluid mechanics: The long way from theoretical models to clinical applications," *Ann. Biomed. Eng.* **43**, 26–40 (2015).
- ³⁵D. Collià and G. Pedrizzetti, "Cardiac fluid dynamics in prolapsed and repaired mitral valve," In: Carcaterra, A., Paolone, A., Graziani, G. (eds) *Proceedings of XXIV AIMETA Conference 2019. AIMETA 2019. Lecture Notes in Mechanical Engineering*. Springer, Cham, **1**, 857–867 (2020).
- ³⁶D. Collià and G. Pedrizzetti, "Cardiac fluid dynamics of patient-specific geometries in pre and post mitral valve repair by direct numerical simulation," In: Accardo, A., Brun, F., Marceglia, S., Pedrizzetti G. (eds) *Seventh National Congress Of Bioengineering Proceeding. GNB 2020*. Patron editore. ISSN 2724-2129 **7**, 12:1–4 (2020).
- ³⁷G. Pedrizzetti, G. Faganello, E. Croatto, and A. D. Lenarda, "The hemodynamic power of the heart differentiates normal from diseased right ventricles," *Journal of Biomechanics* **119**, 110312 (2021).
- ³⁸R. Stegeman, K. D. Lamur, H. Avd, J. M. Breur, F. Groenendaal, and N. J. Jansen, "Neuroprotective drugs in infants with severe congenital heart disease: a systematic review," *Front Neurol* **9**, 521 (2018).
- ³⁹W. T. Mahle, F. Tavani, R. A. Zimmerman, S. C. Nicolson, K. K. Galli, J. W. Gaynor, R. R. Clancy, L. M. Montenegro, T. Spray, and R. M. J. C. Chiavacci, "An mri study of neurological injury before and after congenital heart surgery," *Circulation* **106**, 109–114 (2002).
- ⁴⁰M. Barkhuizen, R. Abella, J. S. H. Vles, L. J. I. Zimmermann, D. Gazzolo, and A. W. D. Gavilanes, "Antenatal and perioperative mechanisms of global neurological injury in congenital heart disease," *Pediatric Cardiology* **42**, 1–18 (2021).
- ⁴¹T. Hansen, T. B. Henriksen, C. C. Bach, and N. B. Matthiesen, "Congenital heart defects and measures of prenatal brain growth: a systematic review," *Pediatr. Neurol.* **72**, 7–18 (2017).
- ⁴²H. Hövels-Gürich, K. Konrad, D. Skorzynski, R. Minkenber, B. Herpertz-Dahlmann, B. Messmer, and M. C. Seghaye, "Long-term behavior and quality of life after corrective cardiac surgery in infancy for tetralogy of fallot or ventricular septal defect," *Pediatr. Cardiol.* **28**, 346–354 (2007).
- ⁴³H. Hövels-Gürich, K. Konrad, D. Skorzynski, C. Nacken, R. Minkenber, B. J. Messmer, and M. C. Seghaye, "Long-term neurodevelopmental outcome and exercise capacity after corrective surgery for tetralogy of fallot or ventricular septal defect in infancy," *Ann. Thorac. Surg.* **81**, 958–966 (2006).
- ⁴⁴R. J. Sommer, Z. M. Hijazi, and J. F. Rhodes Jr, "Pathophysiology of congenital heart disease in the adult - part i: Shunt lesions," *Circulation* **117**, 1090–1099 (2008).
- ⁴⁵G. P. Diller, A. Uebing, K. Willson, L. C. Davies, K. Dimopoulos, S. A. Thorne, M. A. Gatzoulis, and D. P. Francis, "Analytical identification of ideal pulmonary-systemic flow balance in patients with bidirectional cavopulmonary shunt and univentricular circulation: oxygen delivery or tissue oxygenation?" *Circulation* **114**, 1243–1250 (2006).
- ⁴⁶M. E. Pierpont, C. T. Basson, D. W. Benson, B. D. Gelb, T. M. Giglia, E. Goldmuntz, G. McGee, C. A. Sable, D. Srivastava, and C. L. Webb, "A scientific statement from the american heart association congenital cardiac defects committee, council on cardiovascular disease in the young," *Circulation* **115**, 3015–3038 (2007).
- ⁴⁷S. N. Nees and W. K. Chung, "Genetic basis of human congenital heart disease," *Cold Spring Harb Perspect. Biol.* **12**, a036749 (2020).
- ⁴⁸L. K. K. J. K. Peterson and K. G. Catton, J. H. Moller, and S. P. Setty, "Long term outcomes of children with trisomy 13 and 18 after congenital heart disease interventions," *Ann. Thorac. Surg.* **103**, 1941–1949 (2017).